arXiv:1512.06179v4 [cond-mat.supr-con] 18 Jun 2016

What makes the T_c of monolayer FeSe on $SrTiO_3$ so high: a sign-problem-free quantum Monte Carlo study

Zi-Xiang Li[1], Fa Wang[2,3], Hong Yao[1,3,*] & Dung-Hai Lee[4,5,*]
[1]*Institute for Advanced Study, Tsinghua University, Beijing 100084, China.*
[2]*International Center for Quantum Materials, School of Physics, Peking University, Beijing 100871, China.*
[3]*Collaborative Innovation Center of Quantum Matter, Beijing 100871, China.*
[4]*Department of Physics, University of California, Berkeley, CA 94720, USA.*
[5]*Materials Sciences Division, Lawrence Berkeley National Laboratory, Berkeley, CA 94720, USA.*

Monolayer FeSe films grown on $SrTiO_3$ (STO) substrate show superconducting gap-opening temperatures (T_c) which are almost an order of magnitude higher than those of the bulk FeSe and are highest among all known Fe-based superconductors. Angle-resolved photoemission spectroscopy (ARPES) observed "replica bands" suggesting the importance of the interaction between FeSe electrons and STO phonons. These facts rejuvenated the quest for T_c enhancement mechanisms in iron-based, especially iron-chalcogenide, superconductors. Here, we perform the first numerically-exact sign-problem-free quantum Monte Carlo simulations to iron-based superconductors. We (i) study the electronic pairing mechanism intrinsic to heavily electron doped FeSe films, and (ii) examine the effects of electron-phonon interaction between FeSe and STO as well as nematic fluctuations on T_c. Armed with these results, we return to the question "what makes the T_c of monolayer FeSe on $SrTiO_3$ so high?" in the conclusion and discussions.

1. Introductions

The strong Cooper pairing in monolayer FeSe film on $SrTiO_3$ substrate ($(FeSe)_1$/STO) [1] continues to attract a great deal of attentions (e.g. Refs. [2–17]). Recent developments in the study of FeSe-based high temperature superconductors clearly indicate there are at least two factors that are important to the enhancement of T_c from 8.9 K (bulk FeSe) to about 75 K in $FeSe/BaTiO_3/SrTiO_3$ [5]. These factors are (1) heavy electron doping [9–14] and (2) the effects of the substrate [15, 16].

The first factor, namely heavy electron doping, shapes the fermiology into that best for the intrinsic electron pairing mechanism to act [17]. Concerning the intrinsic pairing mechanism there are two main candidates: the spin [18–23] and orbital [24] fluctuations mediated pairing. However, these proposals are based on approximations that are often not controlled in the presence of strong correlations. By now there are mounting experimental [25–27] and theoretical [28–30] evidences that iron-based superconductors, in particular the iron-chalcogenide superconductors, are strongly correlated.

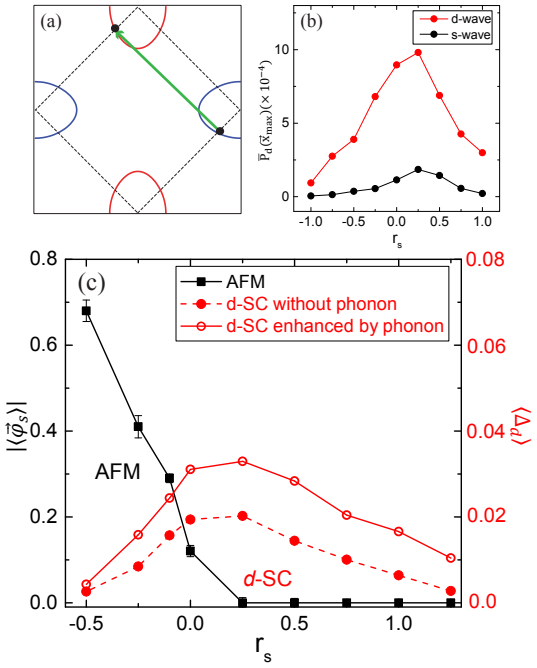

FIG. 1. **a** The Fermi surfaces of the bandstructure used in our simulations. The J_1-type AFM fluctuations can cause the inter-pocket scattering (green arrow). **b** The SC correlation in s- and d-wave pairing channels as a function of the parameter that controls the J_1-type spin fluctuations (the size $L = 18$). **c** The phase diagram for the J_1-type spin fluctuations where the d-wave SC is substantially enhanced by the electron-phonon coupling (solid red curve) compared to the one without electron-phonon couplings (dashed red curve). Here we use the ground state expectation value of the AFM and SC order parameters as a measure of their ordering temperatures

Thus, a theoretical method free of uncontrolled approximations suitable for handling such situation is in high demand.

An experiment that sheds lots of light on the second factor, i.e., the effects of substrate, is the ARPES result of Ref. [15], which shows "replica bands" approximately 100 meV away from all low binding energy bands. Such phenomenon is explained in terms of "phonon shake off", and the phonons are identified with the longitudinal optical phonon branch of STO [15, 16]. This result suggests there is a strong coupling between the FeSe electrons and

STO phonons. Moreover, it is conjectured that such coupling can substantially enhance the T_c intrinsic to heavily electron doped FeSe [15, 16].

In the rest of the paper, we perform large-scale projector quantum Monte Carlo (QMC) [31–33] simulation (details are discussed in Ref. [34]). It turns out that the fermiology, namely the existence of two separate electron Fermi pockets, of $(FeSe)_1$/STO allows the simulation to be free of the fermion minus sign problem. This enables us to perform approximation-free unbiased study of the intrinsic electronic pairing mechanisms, namely, the antiferromagnetic (AFM) and antiferro-orbital (AFO) fluctuation mediated pairing. It also allows us to study the effects of electron-phonon interaction between FeSe and STO [16] and nematic fluctuations [35, 36] on T_c.

A summary of our results is as follows. For the intrinsic pairing mechanisms we have studied two types of spin fluctuations and one type of orbital fluctuations. A commonality between these fluctuations is that they all scatter electrons from one Fermi pocket to the other. (1) For spin fluctuations mimicking the nearest-neighbor AFM exchange interaction (the "J_1-type" spin fluctuation) the ground state exhibits *nodeless* d-wave superconducting (SC) long range order. (2) For spin fluctuations mimicking the next-nearest-neighbor AFM exchange interaction (the "J_2-type"spin fluctuation) the ground state exhibits s-wave SC long range order. (3) The AFO fluctuations trigger s-wave pairing. For the enhancement mechanisms we have studied the small momentum transfer electron-phonon interactions and the nematic fluctuations. Our results clearly show (4) the small momentum transfer electron-phonon interaction significantly strengthens the Cooper pairing triggered by both spin and orbital fluctuations. (5) Similar to the electron-phonon interaction nematic fluctuations also strengthen the Cooper pairing triggered by all three intrinsic mechanisms discussed above. A highlight of some of the main results is shown in Fig. 1.

2. Sign-problem-free quantum Monte Carlo

The effective actions we consider are given in the Supplementary Information I−IV. These actions consist of three parts: (1) the bandstructure of electrons, (2) various fluctuating Bose fields, and (3) the "Yukawa" coupling between the Bose fields and electrons. The bandstructure is chosen to mimic the Fermi surfaces of $(FeSe)_1$/STO as shown in Fig. 1a. We use the one-iron Brillouin zone because it has been shown experimentally that when folded to the corners of the two-iron Brillouin zone the electron pockets show negligible hybridization at their crossings [37].

For intrinsic pairing mechanisms the Bose fields we studied include $\vec{\varphi}_{\rm s}$ and $\varphi_{\rm o}$ associated with the spin and orbital fluctuations respectively. These fields scatter electrons between the Fermi pockets as shown by the green arrow in Fig. 1a. For the pairing enhancement

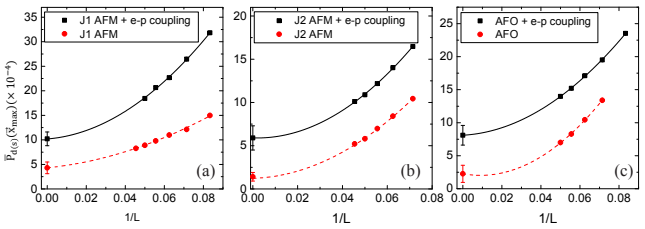

FIG. 2. The enhancement of SC correlation by the small momentum transfer electron-phonon interaction. In each panel the SC correlation in the dominant pairing channel, $\overline{P}_d(L/2, L/2)$, is plot as a function of $1/L$ with and without the electron-phonon interactions. Panels (**a**)−(**c**) are for J_1-type spin (**a**), J_2-type spin (**b**), and AFO (**c**) fluctuations, respectively

mechanisms, we studied STO phonons and nematic fluctuations. The Bose fields associated with them are $\varphi_{\rm ph}$ and $\varphi_{\rm n}$, they cause small momentum transfer (*i.e.* intra-pocket) scattering of the FeSe electrons. The reason we only consider small momentum phonon scattering is due to the forward-focusing nature of the electron-phonon interaction deduced from Ref. [15]. In Eqs. (S2), Eq. (S5) and Eq. (S9), the parameters $r_{\rm s,o,n}$ tune $\vec{\varphi}_{\rm s}$, $\varphi_{\rm o}$, $\varphi_{\rm n}$ across their respective quantum phase transitions. Large negative values correspond to strongly ordered phase and large positive values correspond to the strongly disordered phase. The parameter $r_{\rm ph}$ in Eq. (S7) controls the optical phonon frequency at $\vec{q} = 0$. Remarkably, in all cases our QMC calculation has no minus sign problem [38–40] (see Supplemental Material VI). The QMC simulation is carried out on a square lattice with $N = L \times L$ sites using periodic boundary conditions. In the following we present the simulation results.

3. The spin fluctuation mediated pairing

(1) The J_1-type spin fluctuation: The effective action is given by Eqs. (S1)–(S3). The reason we refer to it as the J_1-type spin fluctuation is because integrating out $\vec{\varphi}_{\rm s}$ generates an AFM exchange interaction whose momentum space coupling constant has the same sign has that of the nearest-neighbor (J_1) AFM exchange interaction. From the Binder cumulant [41] of the AFM order parameter (not shown), we estimate the AFM quantum critical point $r_{\rm s,c}$ to lie in the range of $(0, 0.25)$. To study superconductivity we compute the equal-time pair-pair correlation function $\overline{P}_{s/d}(\vec{x}_{\rm max})$ (see Eqs. (S11)–(S13)). Here s/d denotes s-wave (same sign on the two electron pockets) and (nodeless) d-wave (opposite sign on the two electron pockets) pairing, respectively. $\vec{x}_{\rm max} = (L/2, L/2)$ is the maximum separation between the two pair fields in a system of size L. In Fig. 1b, we plot $\overline{P}_{s/d}(L/2, L/2)$ for $L = 18$ as a function of $r_{\rm s}$. Clearly superconductivity is enhanced near the magnetic quantum critical point.

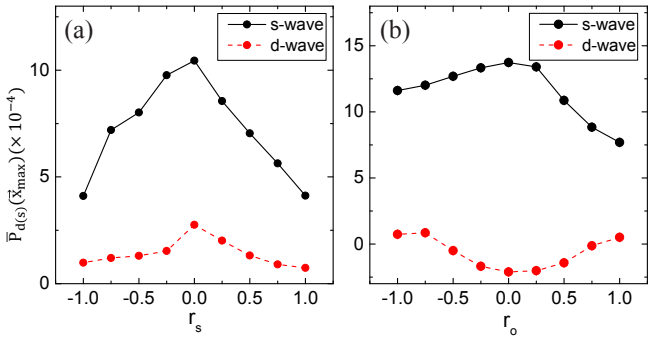

FIG. 3. The SC correlation, $\overline{P}(L/2, L/2)$, in the s- and d-wave pairing channels for $L = 14$ triggered by the (**a**) J_2-type spin and (**b**) AFO fluctuations. For both cases, the s-wave pairing is favored over the d-wave

Moreover, the d-wave pairing is favored over the s-wave [42].

In Fig. 2a (red curve), we show the size-dependence of $\overline{P}_d(L/2, L/2)$ at $r_s = 0.25$ for $L = 12, 14, 16, 18, 20, 22$ (the red points). The red curve is the best fit using a second order polynomial in $1/L$. This allows us to extrapolate to $L \to \infty$ to obtain $\overline{P}_d(L \to \infty) = (4.3 \pm 1.1) \times 10^{-4}$. This establishes the fact that the ground state possesses nodeless d-wave superconducting long-range order!

(2) The J_2-type spin fluctuation: The effective action is given by Eqs. (S1),(S2) and (S4). In this case, integrating out the spin boson $\vec{\varphi}_s$ generates an AFM exchange interaction whose momentum space coupling constant has the same sign has that of the next nearest neighbor (J_2) AFM exchange interaction. From the Binder cumulant (not shown here) we deduce the quantum critical point to be situated within $0.0 \leq r_{s,c} \leq 0.25$. In Fig. 3a, we plot $\overline{P}_{s/d}(L/2, L/2)$ for $L = 14$ as a function of r_s. Here s-wave superconductivity is enhanced near the magnetic quantum critical point.

In Fig. 2b (red curve), we study the size-dependence of $\overline{P}_d(L/2, L/2)$ at $r_s = 0.25$ for $L = 12, 14, 16, 18, 20, 22$ (the red points). The red curve is the best fit using a second order polynomial in $1/L$. This allows us to extrapolate to $L \to \infty$ to obtain $\overline{P}_d(L \to \infty) = (1.4 \pm 0.5) \times 10^{-4}$. This establishes the fact that the ground state possesses nodeless s-wave superconducting long-range order.

4. The AFO fluctuation mediated pairing

In this section, we study the effects of AFO fluctuation (φ_o) on superconductivity. The effective action is given by Eqs. (S1), (S5) and (S6). Like the AFM fields the AFO field also scatters electrons between the two Fermi pockets (the green arrow in Fig. 1a).

From the Binder cumulant associated with the AFO order parameter (not shown here) we deduce the AFO quantum critical point to be situated within $0.0 \leq r_{o,c} \leq 0.25$. In Fig. 3b, we plot $\overline{P}_{s/d}(L/2, L/2)$ for $L = 14$ as a function of r_o. Clearly s-wave superconducting correlation is favored over the d-wave, and it is peaked near the AFO quantum critical point. In Fig. 2c (red curve) we study the size-dependence of $\overline{P}_d(L/2, L/2)$ at $r_o = 0.25$ for $L = 12, 14, 16, 18, 20, 22$ (the red points). The red curve is the best fit using a second order polynomial in $1/L$. This allows us to extrapolate to $L \to \infty$ to obtain $\overline{P}_s(L \to \infty) = (2.1 \pm 0.9) \times 10^{-4}$. This indicates that the ground state possesses s-wave superconducting long-range order.

5. The pairing enhancement due to STO phonons

Motivated by Ref. [15], here we study the effect of small momentum transfer electron-phonon coupling on the superconductivity triggered by pure AFM and AFO fluctuations. This is done by adding the coupling to $\varphi_{\rm ph}$ (see Eqs. (S7), (S8)). The parameter $r_{\rm ph}$ that controls the phonon frequency is fixed at 0.5. The strength of the electron-phonon coupling is controlled by $\lambda_{\rm ph}$. The value of $\lambda_{\rm ph}$ is chosen so that the dimensionless strength of the phonon mediated attraction $\lambda = \frac{\lambda_{\rm ph}^2}{r_{\rm ph} W} = 0.6$. Here W is the electron band width. This value is similar to the estimate given in Ref. [15]. In the following we fix the parameter $r_{s,o}$ at 0.25. In Fig. 2 we compare the size dependence of the superconducting correlation function in the dominant pairing channels with (black curve) and without (red curve) phonons. Clearly the SC order is enhanced by the electron-phonon interaction regardless of the intrinsic pairing mechanisms.

The phase diagram in Fig. 1c is constructed from the extrapolated value of the AFM and SC order parameters from finite-size analysis for each r_s. The plot is for the J_1-type spin fluctuation, however we expect a similar plot holds for J_2-type spin and AFO fluctuations as well. In the phase diagram, we use the ground state expectation value of the AFM and SC order parameters as a measure of their ordering temperatures. It is clear that the SC ordering temperature T_c is enhanced by the electron-phonon couplings for all value of r_s. Remarkably, the T_c enhancement by phonons is largest around the AFM quantum critical point.

In Supplementary Materials VII, we study the enhancement of the superconducting order parameter due to J_1-type spin and AFO fluctuations as a function of the dimensionless phonon-mediated attraction strength λ. Apparently, the enhancement of superconductivity peaks at $\lambda = 1.5$ for the J_1-type spin fluctuation triggered d-wave pairing. For the AFO induced s-wave pairing the pair-pair correlation increases monotonously with the electron-phonon coupling strength up to $\lambda = 2.2$.

6. The pairing enhancement by nematic fluctuations

In view of the possibility that nematic fluctuation can be substantial in heavily electron-doped FeSe films [17], here

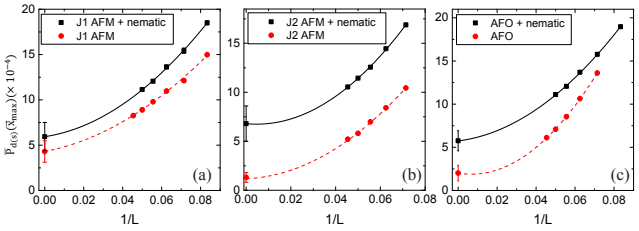

FIG. 4. The enhancement of SC correlation by nematic fluctuations. In each panel, the SC correlation in the dominant pairing channel, $\overline{P}_d(L/2, L/2)$, is plot as a function of $1/L$ with and without the electron phonon interaction. Panels (**a**)−(**c**) are for J_1-type spin (**a**) J_2-type spin (**b**) and AFO (**c**) fluctuations, respectively

we study the effects of nematic fluctuations on superconductivity. The effective action is given by Eqs. (S1),(S9) and (S10).

In Fig. 4, we compare the size dependence of the superconducting correlation function in the dominant pairing channels with (black curve) and without (red curve) nematic fluctuations. Like the electron-phonon interaction, the SC order is enhanced by the nematic fluctuations for all intrinsic pairing mechanisms considered.

7. Conclusion and discussions

A definitive answer to "why T_c is so high in monolayer FeSe on $SrTiO_3$?" requires one to (1) determine the intrinsic pairing mechanisms which is primarily responsible to Cooper pairing in heavily electron doped FeSe-based high temperature superconductors, and (2) pin down the effects of substrate.

Regarding (2), our results show that small momentum transfer electron-phonon scattering enhances superconductivity regardless of whether it is triggered by the spin or orbital fluctuations, hence lend support to the phonon enhancement mechanism discussed in Refs. [15, 16]. However our result holds for all phonons that scatter the FeSe electron with small momentum transfer. It does not allow us to conclude that the particular branch of high frequency phonon which caused the replica bands in Ref. [15] is *solely* responsible for the T_c enhancement. In particular it does not rule out the importance of other lower frequency polar phonons.

Regarding (1), our results do not allow us to answer whether spin or orbital fluctuation is main intrinsic pairing mechanism in heavily electron doped FeSe films. However we can confidently predict the pairing symmetry associated with each pairing mechanism. In particular if the pairing symmetry turns out to be s-wave it can come from several different mechanisms: J_2-type spin fluctuation or anti-ferro orbital fluctuation, or the combination of them with nematic fluctuation. However if the pairing symmetry is d-wave our result uniquely pins down the J_1-type spin fluctuation as the driving force.

Experimentally the pairing symmetry of $(FeSe)_1/STO$ is still an open question. However we would like to list a number of circumstantial evidence that the pairing symmetry might be d-wave. The first is the existence of neutron resonance *below twice the superconducting gap* in materials with similar fermiology [43, 44], and the fact that the momentum locations of the resonance are consistent with inter-pocket scattering. The second is a recent high resolution ARPES study of the superconducting gap anisotropy of $(FeSe)_1/STO$ [37]. It observes four minima in the superconducting gap at the momentum locations corresponding to the crossing of the two Fermi pockets (in the two iron Brillouin zone). This can be interpreted as the result due to weak inter-pocket hybridization on a *nodeless* d-wave gap [45]. Moreover the weakness of the inter-pocket hybridization is evidenced by the lack of splitting at the Fermi pocket crossings in the normal state.

Although there is no direct evidence of strong nematic fluctuation in $(FeSe)_1/STO$ we can not rule out that it does play a partial role in the pairing of heavily electron doped FeSe films. By itself nematic fluctuation will not discriminate between s- and d-wave pairings. However when coupled with the spin or orbital fluctuations it can significantly enhance the pairing strength favored by each of them.

Acknowledgments

We would like to thank the National Supercomputer Center in Guangzhou for computational support. ZXL and HY were supported in part by the National Thousand Young-Talents Program and the National Natural Science Foundation of China (11474175). FW was supported by the National Natural Science Foundation of China(11374018). DHL was supported by the U.S. Department of Energy, Office of Science, Basic Energy Sciences, Materials Sciences and Engineering Division, grant DE-AC02-05CH11231.

Note added.– After our work was posted on arXiv.org, another sign-problem-free QMC on FeSe appeared [46]. However the focus of Ref.[46] is quite different from ours.

Conflict of interest

The authors declare that they have no conflict of interest.

*yaohong@tsinghua.edu.cn, dunghai@berkeley.edu.

[1] Wang QY, Li Z, Zhang WH et al (2012) Interface-induced high-temperature superconductivity in single unit-cell FeSe films on $SrTiO_3$. Chin Phys Lett 29:037402

[2] Liu DF, Zhang WH, Mou DX et al (2012) Electronic origin of high-temperature superconductivity in single-layer FeSe superconductor. Nat Commun 3:931

[3] Tan Sy, Zhang Y, Xia M et al (2013) Interface-induced superconductivity and strain-dependent spin density waves in FeSe/$SrTiO_3$ thin films. Nat Mater 12:634–640

[4] He SL, He JF, Zhang WH et al (2013) Phase diagram and electronic indication of high-temperature superconductivity at 65 K in single-layer FeSe films. Nat Mater 12:605-610

[5] Peng R, Xu HC, Tan SY et al (2014) Tuning the band structure and superconductivity in single-layer FeSe by interface engineering. Nat Commun 5:5044

[6] Ge JF, Liu ZL, Liu C et al (2015) Superconductivity above 100 K in single-layer FeSe films on doped $SrTiO_3$. Nat Mater 14:285

[7] Zhang Z, Wang YH, Song Q et al (2015) Onset of the Meissner effect at 65 K in FeSe thin film grown on Nb-doped $SrTiO_3$ substrate. Sci Bull 60:1301–1304

[8] Tang C, Zhang D, Zang Y et al (2015) Superconductivity dichotomy in K-coated single and double unit cell FeSe films on $SrTiO_3$ Phys Rev B 92:180507

[9] Lu XF, Wang NZ, Wu H et al (2015) Coexistence of superconductivity and antiferromagnetism in $(Li_{0.8}Fe_{0.2})$OHFeSe. Nat Mater 14:325–329

[10] Zhao L, Liang AJ, Yuan DN et al (2016) Common electronic origin of superconductivity in (Li,Fe)OHFeSe bulk superconductor and single-layer FeSe/$SrTiO_3$ Films. Nat Commun 7:10608

[11] Niu XH, Peng R, Xu HC et al (2015) Surface electronic structure and isotropic superconducting gap in (Li_0.8Fe_0.2)OHFeSe. Phys Rev B 92: 060504

[12] Miyata Y, Nakayama K, Sugawara K et al (2015) High-temperature superconductivity in potassium-coated multilayer FeSe thin films. Nat Mater 14:775–779

[13] Wen CHP, Xu HC, Chen C et al (2016) Anomalous correlation effects and unique phase diagram of electron doped FeSe revealed by angle resolved photoemission spectroscopy. Nat Commun 7:10840

[14] Tang C, Liu C, Zhou G et al (2016) Interface enhanced electron-phonon coupling and high temperature superconductivity in potassium-coated ultra-thin FeSe films on $SrTiO_3$. Phys Rev B 93:020507

[15] Lee JJ, Schmitt FT, Moore RG et al (2014) Interfacial mode coupling as the origin of the enhancement of T_c in FeSe films on $SrTiO_3$. Nature 515:245-248

[16] Lee DH (2015) What makes the T_c of FeSe/$SrTiO_3$ so high? Chin Phys B 24:117405

[17] Ye ZR, Zhang CF, Ning HL et al (2015) Simultaneous emergence of superconductivity, inter-pocket scattering and nematic fluctuation in potassium-coated FeSe superconductor. arXiv:1512.02526

[18] Mazin II, Singh DJ, Johannes MD et al (2008) Unconventional superconductivity with a sign reversal in the order parameter of $LaFeAsO_{1-x}F_x$. Phys Rev Lett 101:057003

[19] Kuroki K, Onari S, Arita R et al (2008) Unconventional pairing originating from the disconnected Fermi surfaces of superconducting $LaFeAsO_{1-x}F_x$. Phys Rev Lett 101:087004

[20] Chubukov AV, Efremov DV, Eremin I (2008) Magnetism, superconductivity, and pairing symmetry in iron-based superconductors. Phys Rev B 78:134512

[21] Seo K, Bernevig BA, Hu J (2008) Pairing symmetry in a two-orbital exchange coupling model of oxypnictides. Phys Rev Lett 101:206404

[22] Wang F, Zhai H, Ran Y et al (2009) Functional renormalization-group study of the pairing symmetry and pairing mechanism of the FeAs-based high-temperature superconductor. Phys Rev Lett 102:047005

[23] Graser S, Maier TA, Hirschfeld PJ et al (2009) Near-degeneracy of several pairing channels in multiorbital models for the Fe-pnictides. New J Phys 11:025016

[24] Kontani H, Onari S (2010) Orbital-fluctuation-mediated superconductivity in iron pnictides: analysis of the five-orbital Hubbard-Holstein model. Phys Rev Lett 104:157001

[25] Qazilbash MM, Hamlin JJ, Baumbach RE et al (2009) Electronic correlations in the iron pnictides. Nat Phys 5:647–650

[26] Tamai A, Ganin AY, Rozbicki E et al (2010) Strong electron correlations in the normal Sstate of the iron-based $FeSe_{0.42}Te_{0.58}$ superconductor observed by angle-resolved photoemission spectroscopy. Phys Rev Lett 104:097002

[27] Yi M, Liu ZK, Zhang Y et al (2015) Observation of universal strong orbital-dependent correlation effects in iron chalcogenides. Nat Commun 6:7777

[28] Si Q, Abrahams E, Dai J et al (2009) Correlation effects in the iron pnictides. New J Phys 11:045001

[29] Yin ZP, Haule K, Kotliar G (2011) Kinetic frustration and the nature of the magnetic and paramagnetic states in iron pnictides and iron chalcogenides. Nat Mater 10:932

[30] Georges A, de'Medici L, Mravlje J (2013) Strong correlations from Hund's coupling. Annual Review of Condensed Matter Physics 4:137

[31] Sorella S, Baroni S, Car R et al (1989) A novel technique for the simulation of interacting fermion systems. Europhys Lett 8:663

[32] White SR, Scalapino DJ, Sugar RL et al (1989) Numerical study of the two-dimensional Hubbard model. Phys Rev B 40:506

[33] Assaad FF, Evertz HG (2008) World-line and determinantal quantum Monte Carlo methods for spins, phonons and electrons. In Computational many-prticle physics, Fehske H, Schneider R, Weiβe, A (Eds.). 277-356 (Lecture Notes in Physics, 2008)

[34] Li ZX, Wang F, Yao H et al (2015) The nature of effective interaction in cuprate superconductors: a sign-problem-free quantum Monte-Carlo study. arXiv:1512.04541

[35] Lederer S, Schattner Y, Berg E et al (2015) Enhancement of superconductivity near a nematic quantum critical point. Phys Rev Lett 114:097001

[36] Schattner Y, Lederer S, Kivelson SA et al (2015) Ising nematic quantum critical point in a metal: a Monte Carlo study. arXiv:1511.03282

[37] Zhang Y, Lee JJ, Moore RG et al (2015) Superconducting gap anisotropy in monolayer FeSe thin film. arXiv:1512.06322

[38] Wu C, Zhang SC (2005) Sufficient condition for absence of the sign problem in the fermionic quantum Monte Carlo algorithm. Phys Rev B 71:155115

[39] Berg E, Metlitski MA, Sachdev S (2012) Sign-problem-free quantum Monte Carlo of the onset of antiferromagnetism in metals. Science 338:1606

[40] Li ZX, Jiang YF, Yao H (2015) Solving the fermion sign problem in quantum Monte Carlo simulations by Majorana representation. Phys Rev B 91:241117

[41] Binder K (1981) Finite size scaling analysis of Ising model block distribution functions. Zeitschrift fur Physik B Condensed Matter 43:119–140

[42] Davis JCS, Lee DH (2013) Concepts relating magnetic interactions, intertwined electronic orders, and strongly correlated superconductivity. PNAS 110:17623–17630

[43] Park JT, Friemel G, Li Y et al (2011) Magnetic resonant mode in the low-energy spin-excitation spectrum of superconducting $Rb_2Fe_4Se_5$ single crystals. Phys Rev Lett 107:177005

[44] Friemel G, Liu WP, Goremychkin EA et al (2012) Conformity of spin fluctuations in alkali-metal iron selenide superconductors inferred from the observation of a magnetic resonant mode in $K_xFe_{2-x}Se_2$. Europhys Lett 99:67004

[45] Mazin II (2011) Symmetry analysis of possible superconducting states in $K_xFe_ySe_2$ superconductors. Phys Rev B 84:024529

[46] Dumitrescu PT, Serbyn M, Scalettar RT et al (2015) Superconductivity and Nematic Fluctuations in a model of FeSe monolayers: A Determinant Quantum Monte Carlo Study. arXiv:1512.08523.

SUPPLEMENTAL MATERIALS

I. The effective action for the J_1 and J_2 types of spin fluctuations

The effective action, based on a two band model describing band structure of single-layer $(FeSe)_1$/STO, is given by $S = S_F + S_s$ where $S_s = S_B + S_{FB}$ and

$$S_F = \int_0^\beta d\tau \sum_{jk,\alpha=x,y} \psi^\dagger_{j\alpha}\big[(\partial_\tau - \mu)\delta_{jk} - t_{jk,\alpha}\big]\psi_{k\alpha}, \tag{S1}$$

$$S_B = \int_0^\beta d\tau\Big\{\frac{1}{2}\sum_j \frac{1}{c_s^2}|\partial_\tau\vec{\varphi}_{s,j}|^2 + \frac{1}{2}\sum_{\langle jk\rangle}|\vec{\varphi}_{s,j} - \vec{\varphi}_{s,k}|^2 + \sum_j\Big[\frac{r_s}{2}|\vec{\varphi}_{s,j}|^2 + \frac{u_s}{4}\left(|\vec{\varphi}_{s,j}|^2\right)^2\Big]\Big\}, \tag{S2}$$

where

$$S_{FB} = \lambda_s\int_0^\beta d\tau\sum_j(-1)^j\Big[\psi^\dagger_{jx}(\vec{\sigma}\cdot\vec{\varphi}_{s,j})\psi_{jy} + h.c.\Big], \tag{S3}$$

for J_1-type of spin fluctuations. If the spin fluctuation is J_2 type

$$S_{FB} = i\ \lambda_s\int_0^\beta d\tau\sum_j(-1)^j\Big[\psi^\dagger_{jx}(\vec{\sigma}\cdot\vec{\varphi}_{s,j})\psi_{jy} + h.c.\Big]. \tag{S4}$$

In the above equations, j, k labels the sites of a square lattice, $\alpha = x, y$ labels the two orbitals (which transform into each other under the 90 ° rotation) from which the red and blue Fermi surfaces in Fig. 1a of the main text are derived from, τ denotes the imaginary time and β is the inverse temperature. In Eq. (S2), $\vec{\varphi}_s$ is the AFM collective mode and the operator $\psi_{i\alpha}$ is a spinor operator which annihilates an electron in orbital α and on site i. The three $\vec{\sigma}$ are the spin Pauli matrices. It is important to note that in Eq. (S4) the fermion-boson coupling has an extra factor i.

The parameters in this effective action include r_s which tunes the system across the AFM phase transition, c_s is the spin-wave velocity and u_s is the self-interactions of $\vec{\varphi}_s$. λ_s is the "Yukawa" coupling between electrons and AFM order parameter. In our computation, we fix $c_s = u_s = \lambda_s = 1.0$ and vary the value of r_s to control the severity of AFM fluctuation. In the fermion action the hopping integral t_{ij} is chosen to be among nearest neighbor sites and equal to $t_\parallel = 1.0$ for $x(y)$-orbital along $x(y)$ direction and $t_\perp = -0.5$ for $y(x)$ orbital along $x(y)$ direction. We fix the occupancy in our computation to be 0.1 such that the Fermi surface is shown in Fig. 1a of the main text.

II. The effective action for antiferro-orbital fluctuations

The AFO effective action is given by $S = S_F + S_o$ where S_F is the same as in Eq.(S1), $S_o = S_B + S_{FB}$ and

$$S_B = \int_0^\beta d\tau\Big\{\frac{1}{2}\sum_i \frac{1}{c_o^2}|\partial_\tau\varphi_{o,i}|^2 + \frac{1}{2}\sum_{\langle ij\rangle}|\varphi_{o,i} - \varphi_{o,j}|^2 + \sum_i\Big[\frac{r_o}{2}(\varphi_{o,i})^2 + \frac{u_o}{4}\left(\varphi_{o,i}\right)^4\Big]\Big\}, \tag{S5}$$

$$S_{FB} = \lambda_o\int_0^\beta d\tau\sum_i(-1)^i\Big[\varphi_{o,i}\psi^\dagger_{ix}\sigma_0\psi_{iy} + h.c.\Big]. \tag{S6}$$

In Eq. (S6), φ_o is the AFO order parameter and σ_0 is the identity matrix in the spin space.

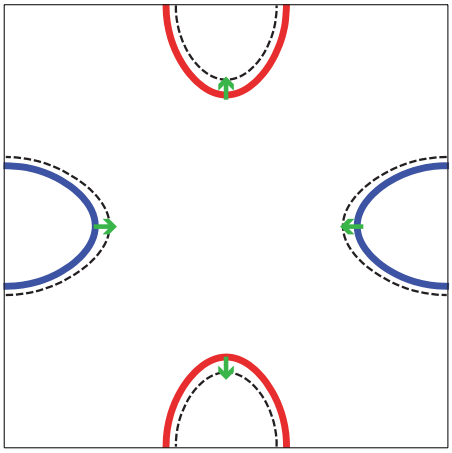

FIG. S1. Dashed lines represent the nematically distorted Fermi surfaces

The parameters in this effective action include the orbital wave velocity $c_{\rm o}$, and $r_{\rm o}$ which tunes the system across the AFO phase transition, and $u_{\rm o}$ is the self-interactions of the $\varphi_{\rm o}$ field. $\lambda_{\rm o}$ is the Yukawa coupling between electrons and AFO order parameter. In our computation, we fix $c_{\rm o} = u_{\rm o} = \lambda_{\rm o} = 1.0$ and vary the value of $r_{\rm o}$ to control the severity of AFO fluctuation.

III. The electron-phonon effective action

The electron-phonon effective action is given by $S = S_{\rm F} + S_{\rm ph}$ where $S_{\rm ph} = S_{\rm B} + S_{\rm FB}$ and

$$S_B = \int_0^\beta {\rm d}\tau \Big\{ \frac{1}{2} \sum_i \frac{1}{c_{\rm ph}^2} |\partial_\tau \varphi_{{\rm ph},i}|^2 + \frac{1}{2} \sum_{\langle ij \rangle} |\varphi_{{\rm ph},i} - \varphi_{{\rm ph},j}|^2 + \sum_i \Big[\frac{r_{\rm ph}}{2} |\varphi_{{\rm ph},i}|^2 \Big] \Big\}, \tag{S7}$$

$$S_{\rm FB} = \lambda_{\rm ep} \int_0^\beta {\rm d}\tau \sum_i \varphi_{{\rm ph},i} \Big[\psi_{ix}^\dagger \sigma_0 \psi_{ix} + \psi_{iy}^\dagger \sigma_0 \psi_{iy} \Big]. \tag{S8}$$

Here $\varphi_{\rm ph}$ is the phonon field, $r_{\rm ph}$ is the frequency of the optical phonon at $\vec{q} = 0$ and $c_{\rm ph}$ is velocity of phonon. We fix parameters $r_{\rm ph} = 0.5, c_{\rm ph} = 1.0$ and vary the value of $\lambda_{\rm ep}$ to tune the strength of electron-phonon coupling.

IV. The effective action for nematic fluctuations

In Fig. S1, we show how does the nematic order parameter distort the Fermi surfaces. The nematic effective action is given by $S = S_{\rm F} + S_{\rm n}$ where $S_{\rm n} = S_{\rm B} + S_{\rm FB}$ and

$$S_{\rm B} = \int_0^\beta {\rm d}\tau \Big\{ \frac{1}{2} \sum_i \frac{1}{c_{\rm n}^2} |\partial_\tau \varphi_{{\rm n},i}|^2 + \frac{1}{2} \sum_{\langle ij \rangle} |\varphi_{{\rm n},i} - \varphi_{{\rm n},j}|^2 + \sum_i \Big[\frac{r_{\rm n}}{2} |\varphi_{{\rm n},i}|^2 + \frac{u_{\rm n}}{4} \varphi_{{\rm n},i}^4 \Big] \Big\}, \tag{S9}$$

$$S_{\rm FB} = \lambda_{\rm n} \int_0^\beta {\rm d}\tau \sum_i \varphi_{{\rm n},i} \Big[\psi_{ix}^\dagger \sigma_0 \psi_{ix} - \psi_{iy}^\dagger \sigma_0 \psi_{iy} \Big]. \tag{S10}$$

In Eq. (S10), $\varphi_{\rm n}$ is the nematic order parameter. The parameters in this effective action include the velocity $c_{\rm n}$, and $r_{\rm n}$ which tunes the system across the nematic phase transition, and $u_{\rm n}$ is the self-interactions of the $\varphi_{\rm n}$ field. $\lambda_{\rm n}$ is the Yukawa coupling between electrons and nematic order parameter. In our computation, we fix $c_{\rm n} = u_{\rm n} = \lambda_{\rm n} = 1.0$ and vary the value of $r_{\rm n}$ to control the severity of nematic fluctuation.

V. The superconducting pair correlation function

To investigate superconductivity we calculate the equal time pair-pair correlation functions

$$P_{s/d}(\vec{r}_i) = \langle \Delta_{s/d}(\vec{r}_i)\Delta^{\dagger}_{s/d}(\vec{0})\rangle, \tag{S11}$$

where

$$\Delta_{s/d}(\vec{r}_i) = \psi^{\mathrm{T}}_{ix}(i\sigma_y)\psi_{ix} \pm \psi^{\mathrm{T}}_{iy}(i\sigma_y)\psi_{iy}, \tag{S12}$$

are the s (+ sign) and d (− sign) wave Cooper pair operators, respectively. To determine whether there is long-range order we put $\vec{r}_i$ to the maximum separation $\vec{x}_{\max}$ of the pair fields (for a system with linear dimension L the value of $\vec{x}_{\max}$ is $(L/2, L/2)$. Moreover, in order to minimize statistical errors, we average the correlation function over 25 sites around $\vec{x}_{\max}$. Thus the actual pair correlation we study is

$$\overline{P}_{d(s)}(\vec{x}_{\max}) = \frac{1}{25}\sum_{n,m=0,\pm1,\pm2} P_{d(s)}(\vec{x}_{\max} + n\hat{x} + m\hat{y}). \tag{S13}$$

VI. Effective actions that are amenable to sign-problem-free QMC simulation

The actions that are amenable to sign-problem-free QMC simulations are any mixture of $S_{\mathrm{F}} + c_1 S_s + c_2 S_{\mathrm{ph}} + c_3 S_{\mathrm{n}}$ and $S_{\mathrm{F}} + c_1 S_o + c_2 S_{\mathrm{ph}} + c_3 S_{\mathrm{n}}$ where $c_{1,2,3} = 0, 1$. Note, however, for S_{s} we can use either J_1 or J_2 type spin fluctuation actions but not both.

Aside from the square lattice spatial symmetries the action $S_{\mathrm{F}} + c_1 S_s + c_2 S_{\mathrm{ph}} + c_3 S_{\mathrm{n}}$ is invariant under the anti-unitary transformation $U = \tau_z(i\sigma_y)K$ and the action $S_{\mathrm{F}} + c_1 S_o + c_2 S_{\mathrm{ph}} + c_3 S_{\mathrm{n}}$ is invariant under $U' = i\sigma_y K$. Here τ_z is the third Pauli matrix acting in orbital (x, y) space and K denotes complex conjugation. It can be shown that because of these symmetries, the fermion determinant for arbitrary Bose fields configuration is positive hence the QMC simulation is free of minus-sign. This enables us to perform large-scale projector QMC simulation. The anti-unitary symmetry $U = \tau_z(i\sigma_y)K$ is the same as that in Ref. [1].

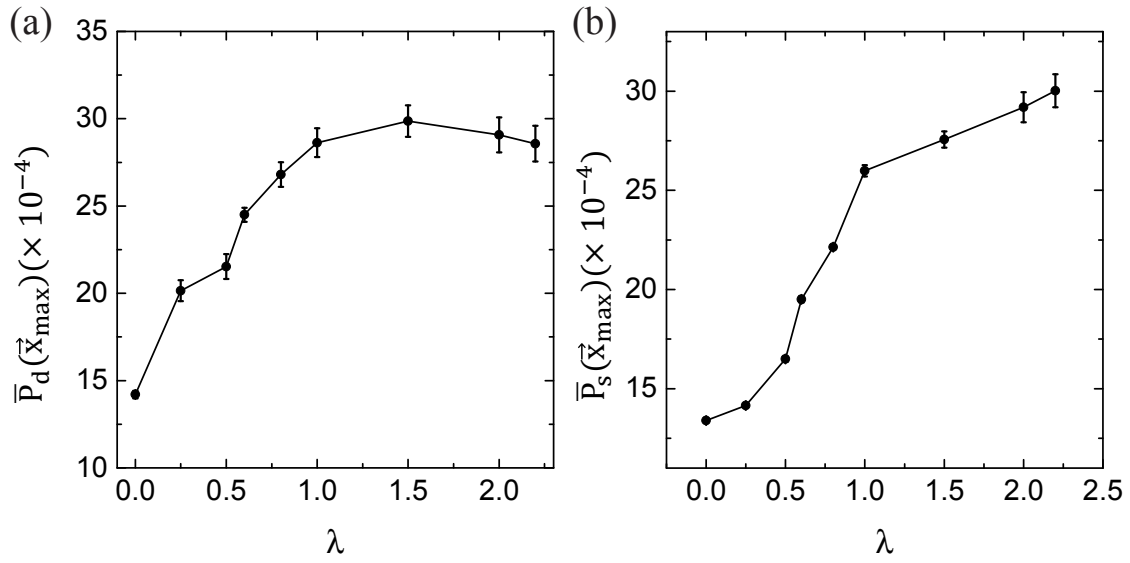

FIG. S2. Enhancement of pairing by electron-phonon coupling. **a** The J_1-type spin fluctuation triggered $\overline{P}_d(L/2, L/2)$ as a function of λ for $L = 14$. **b** The AFO fluctuation triggered $\overline{P}_s(L/2, L/2)$ as a function of λ for $L = 14$

VII. The enhancement of superconductivity triggered by the J_1 spin and AFO fluctuations as a function of the electorn-phonon coupling

In this section, we examine the enhancement of the SC order parameters triggered by the J_1 type spin and AFO fluctuations as a function of the dimensionless electron-phonon coupling strength λ.

In Fig. S2a and b, we plot the enhancement of spin fluctuation induced $\overline{P}_d(L/2, L/2)$ and orbital fluctuation induced $\overline{P}_s(L/2, L/2)$ as a function of λ for $L = 14$. Apparently the enhancement of superconductivity peaks at $\lambda \sim 1.5$ for the J_1-type spin fluctuation triggered d-wave pairing. For the AFO induced s-wave pairing the pair correlation increases monotonously with the amplitude of electron-phonon coupling up to the maximum value of λ we studied (=2.2).

[1] Berg E, Metlitski MA, Sachdev S (2012) Sign-problemCfree quantum Monte Carlo of the onset of antiferromagnetism in metals. Science 338:1606–1609

[2] Sorella S, Baroni S, Car R et al (1989) A novel technique for the simulation of interacting fermion systems. Europhys Lett 8:663

[3] White SR, Scalapino DJ, Sugar RL et al (1989) Numerical study of the two-dimensional Hubbard model. Phys Rev B 40:506

[4] Blankenbecler R, Scalapino DJ, Sugar R L (1981) Monte Carlo calculations of coupled boson-fermion systems. Phys Rev D 24:2278

[5] Assaad FF, Evertz HG (2008) World-line and determinantal quantum Monte Carlo methods for spins, phonons and electrons. In Computational many-prticle physics, Fehske H, Schneider R, Weiβe, A (Eds.). 277-356 (Lecture Notes in Physics, 2008)